REPORT DOCUMENTATION PAGE

Form Approved
OMB No.
~~0704-0188~~

1. AGENCY USE ONLY *(Leave blank)*	2. REPORT DATE	3. REPORT TYPE AND DATES COVERED
	January 2001	Final Technical (11/01/97 - 09/30/00)

4. TITLE AND SUBTITLE
"Wideband Transferred-Substrate AlGaN-GaN Heterojunction Bipolar Transistors for Microwave Power Applications"

5. FUNDING NUMBERS
N00014-98-1-0061

6. AUTHOR(S)
Dr. Umesh K. Mishra / Dr. Lee McCarthy

7. PERFORMING ORGANIZATION NAME(S) AND ADDRESS(ES)
University of California, Santa Barbara, CA 93106

8. PERFORMING ORGANIZATION REPORT NUMBER

9. SPONSORING/MONITORING AGENCY NAME(S) AND ADDRESS(ES)
Office of Naval Research
Program Officer John C. Zolper ONR 312
800 North Quincy Street
Arlington, VA 22217-5660

10. SPONSORING/MONITORING AGENCY REPORT NUMBER

11. SUPPLEMENTARY NOTES

12a. DISTRIBUTION/AVAILABILITY STATEMENT
Distribution Unlimited, approved for public release.

12b. DISTRIBUTION CODE

13. ABSTRACT *(Maximum 200 words)*

This report reviews efforts to develop growth and fabrication technology for the GaN HBT at UCSB. Conventional devices are grown by plasma assisted MBE on MOCVD GaN templates on sapphire and fully MOCVD devices. HBTs were also fabricated on LEO material identifying threading disclocations as the primary source of collector-emitter leakage which was reduced by 4 orders of magnitude for devices on non-dislocated material. Base doping studies show that the mechanism of this leakage is localized punch-through caused by compensation near the dislocation. The cause of the large offset voltage in common emitter characteristics is discussed. The Mg memory effect in MOCVD grown GaN HBTs is investigated and MBE grown device layers are shown to produce sharp doping profiles. The low current gain of these devices, (3-6) is discussed. An air bridge and etch back process is used to fabricate transistors compatible with RF testing. The devices had a common emitter differential current gain of 3.5 with a short circuit current gain cutoff frequency of 2 GHz and an emitter current density of over 6 kA/cm^2. Remaining issues are high base resistance, low current gain, and emitter mesa etch process development.

14. SUBJECT TERMS
GaN HBT, dislocation leakage, grading

15. NUMBER OF PAGES
9

16. PRICE CODE

17. SECURITY CLASSIFICATION OF REPORT	18. SECURITY CLASSIFICATION OF THIS PAGE	19. SECURITY CLASSIFICATION OF ABSTRACT	20. LIMITATION OF ABSTRACT
UNCLASSIFIED	UNCLASSIFIED	UNCLASSIFIED	UL

I. Introduction

THE past several years have seen a dramatic increase in research of GaN materials and devices. Progress has been made in areas including RF electronic devices such as FETs[1] and bipolar transistors [2], [3], [4], [5], as well as optoelectronics devices including light emitters, lasers[6] and detectors[7]. GaN is desirable for electronics applications due to saturated electron velocities of 2×10^7 cm/s[8], and its 3.4 eV bandgap which leads to a critical breakdown field of 2 MV/cm[9], and stability at high temperatures. As demonstrated in other III-V material systems, HBTs offer several important advantages over FETs. HBTs generally have better threshold uniformity and device linearity, as well as lower phase noise than FETs. In addition, the HBT structure inherently offers a higher ratio of output current to parasitic capacitance.

There have been several reports of GaN HBTs in the literature[2], [3], [4], [5], but the results are still preliminary. The fundamental material properties described in Table I can be used in comparison with a mature material system to predict potential RF performance of these devices. Lee et al demonstrated AlInAs/GaInAs HBTs using a transferred substrate Schottky collector technology with a power gain cut-off frequency, f_{max}, of 820 GHz [10]. If this technology were applied to a GaN bipolar structure with a 50 nm base, having a base carrier concentration of 5×10^{19} cm^{-3}, and a 100 nm thick collector, the predicted f_{max} is 200 GHz with a current gain cut-off frequency, f_t, of 200 GHz, and a 15V breakdown voltage. For power switching applications, material properties suggest that a 1 kV device with a collector thickness of 7μm, and a base thickness of 200 nm would have an f_t of 6 GHz and an f_{max} over 300 GHz. This paper presents many of the relevant issues to the development of the GaN bipolar transistor. We discuss the progress and current status of GaN bipolar growth and processing technologies, and suggest future directions for the realization of RF device performance in the HBT.

TABLE I
COMPARISON OF MATERIAL PROPERTIES RELEVANT TO RF PERFORMANCE

Property	*GaN*	*GaInP*	*Si*
v_{sat} [cm/s]	20×10^6	10×10^6	6×10^6
E_{crit} [MV/cm]	2	0.6	0.3

II. Device Details

A typical device structure used in these experiments along with a simulated band diagram is shown in Figure 1. Device structures are grown by plasma assisted MBE on MOCVD GaN templates on sapphire. The use of MBE vs. MOCVD growth for the active layers is discussed in section VIII. The emitter is $Al_{0.1}Ga_{0.9}N$:Si ($N_D=10^{18}$ cm^{-3}) with a GaN:Si emitter contact layer. The base layer is 100 nm GaN:Mg, $N_A=5\times10^{19}$ cm^{-3}. Magnesium is a deep acceptor, $E_A-E_V \approx 110-200$ meV[11], resulting in a carrier concentration of $p=8\times10^{17}$ cm^{-3} for this acceptor density. The collector is 500 nm unintentionally doped (UID) GaN with a background donor concentration of 5×10^{16} cm^{-3}. The subcollector is GaN:Si, $N_D=10^{18}$ cm^{-3}.

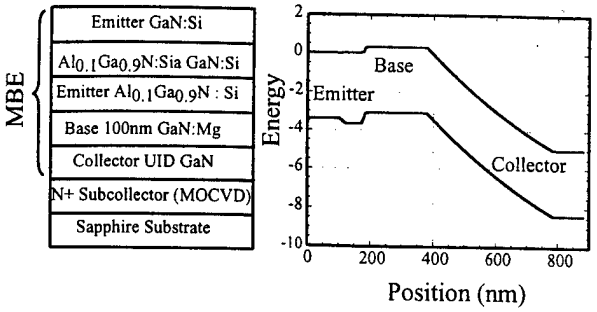

Fig. 1. Left: Typical structure for AlGaN/GaN HBT grown by plasma assisted MBE on MOCVD GaN on sapphire. The collector is unintentionally doped (UID) GaN $N_D\approx 5\times10^{16}cm^{-3}$. Right: Simulated band diagram of typical device. The $Al_{0.1}Ga_{0.9}N$ heterojunction provides 10kT barrier to hole injection into the emitter.

Emitter and collector contacts are Ti/Al/Ni/Au, while the base contacts are Pd/Au. For conventional devices, the mesas are etched with a chlorine reactive ion etch(RIE).

Although there are reports of higher hole concentrations using co-doping of Mg with oxygen or silicon[12], electronic device results with this doping technology have not been reported. Holes in GaN, with an effective mass of $2.2\cdot m_0$[13], have mobilities between 5 and 20 cm^2/V s in highly doped GaN:Mg layers. Consequently, the base of an NPN transistor has a resistivity on the order of 1Ω cm, with a sheet resistivity for a 100 nm base of 100k$\Omega/\Box$. This low base conductivity increases the parasitic base resistance, R_{BB}, degrading RF performance and contributing to the current-crowding effect in the base-emitter junction. In addition, the p-GaN surface is sensitive to etch damage. The Cl_2 RIE used to access the base layer is primarily physical, and is believed to cause point defects, creating states donors, degrading contacts to etched p-type GaN. Although contact resistances as low as $2\times10^{-5}\Omega\cdot cm^{-2}$[14] have been reported on p-type GaN, contacts to Cl_2-RIE etched p-GaN shown in Figure 2 have a voltage barrier of 10V.

The regrown base HBT reduces the contact voltage barrier to the p-GaN surface (Figure 2). After the RIE emitter mesa etch, the emitter is capped with a dielectric mask, AlN_x. In addition to protecting the emitter mesa during the MOCVD growth, the AlN_x mask is selective to GaN growth, and chemically inert in the reducing NH_3+H_2 environment. The etch damage is buried with the new GaN:Mg growth, resulting in an improvement in contact quality as well as increased base conductivity. Used in conjunction with a low-etch-damage RIE process, the base contact voltage barrier is as low as 1V (Figure 2). A further improvement in base-contact quality is attainable with the regrown emitter HBT IV.

III. Offset Voltage

The effect of the poor base conductivity and contact voltage barrier is apparent in the common emitter offset voltage. The offset voltage is the collector-emitter voltage in the common emitter mode where the net collector current becomes positive. At this point, both the base-emitter and base-collector diodes are forward biased. The collector current saturates as the base-collector diode becomes reverse biased. The parasitic offset

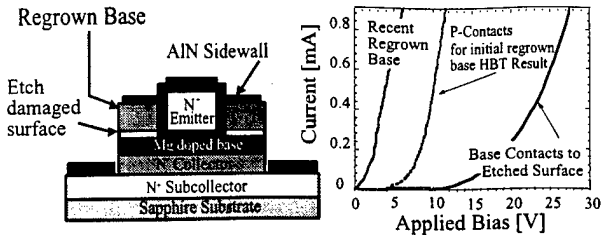

Fig. 2. Comparison showing the improvement resulting from a combination of a less-damaging etch and a regrown extrinsic base.

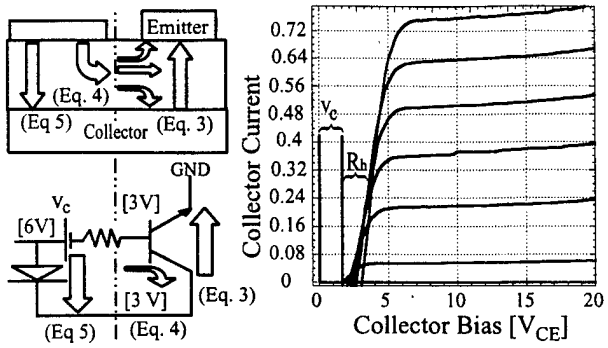

Fig. 3. Large parasitic offset is due to the voltage drop associated with lateral base current. The numbered arrows in the schematic (above left) refer to equations which describe them. The voltages in the wiring diagram (below left) are examples of a bias condition in which the parasitic base-collector diode is forward biased, while the intrinsic device is zero-biased. This is the mechanism for the parasitic offset voltage observed in GaN HBTs.

voltage observed in the GaN HBT is explained as follows:

Because of a high voltage drop across the base contact and a high lateral resistance, the voltage of the base layer under the contact is substantially higher than the voltage of the base in the active device Figure 3). This effectively divides the area under the emitter and the area under the base contact into two devices - the active transistor and a parasitic base-collector diode. The difference between the base voltage under the base contact and the base voltage under the emitter mesa at any given base injection current is the parasitic offset voltage of the transistor. For example, it may require a 6V base emitter contact voltage to inject a 100 μA base current. While the base-emitter junction forward bias is limited by the bandgap to 3.4V, the base voltage under the base contact is $\approx$ 6V. If the collector-emitter voltage is 3.4V, the base-collector diode under the base contact is then forward biased even while the base-collector junction under the emitter mesa is zero-biased (Figure 3). Also, because the contact characteristic is nonlinear, the voltage drop across the contact varies strongly with current density. This leads to a much larger voltage drop across the portion of the contact contributing to the lateral current which feeds the active transistor. This is indicated in Figure 3 as a 'battery' element. The following are equations for the collector current components in an HBT relevant to the common emitter offset voltage:

$$V_{\text{offset}} \equiv V_{CE}\Big|_{I_C=0} \tag{1}$$

$$I_{C_{\text{total}}} = I_{CE} - I_{BC_i} - I_{BC_x} \tag{2}$$

$$I_{CE} = \alpha \cdot A_{\text{emitter}} \cdot J_{s\ BE} \cdot \exp\left[\frac{V_{BE}}{V_T}\right] \tag{3}$$

If $V_{CB_{\text{intrinsic}}} \neq V_{CB_{\text{extrinsic}}}$

$$I_{BC_i} = A_{\text{intrinsic}} \cdot J_{s\ BC} \cdot \exp\left[\frac{V_{BC_i}}{V_T}\right] \tag{4}$$

$$I_{BC_x} = A_{\text{extrinsic}} \cdot J_{s\ BC} \cdot \exp\left[\frac{V_{BC_x}}{V_T}\right] \tag{5}$$

Here we use α as an overall efficiency term that includes emitter injection efficiency as well as the transport efficiency across the base. Equations (4) and (5) split from a single equation when the external base-collector bias differs from the internal bias. In this case, a higher voltage is required to turn off the extrinsic base collector diode. Figure 3 shows the contributions of the offset voltage equations to the total collector current, I_C. Analysis of a measured common emitter characteristic (Figure 3) show these effects on the DC performance. To reduce this offset voltage, the base contact and lateral resistances must be reduced- or the extrinsic collector eliminated as in the transferred substrate Schottky collector technology[10].

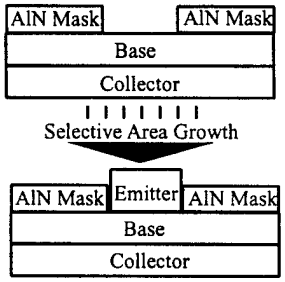

Fig. 4. The selective emitter regrowth step is shown above. The AlN_X mask is used to protect the base surface. The emitter structure is then selectively grown by MOCVD to form emitter mesas. Later, the mask is removed, and the base mesa is etched by Cl_2 RIE. Finally, base, emitter, and collector metalizations are applied using standard lift-off lithographic techniques.

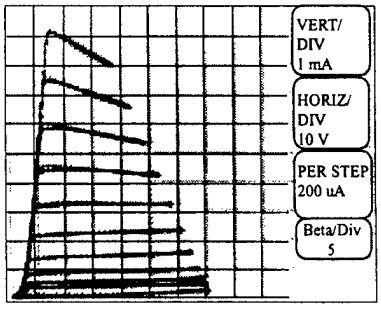

Fig. 5. Common emitter characteristics of regrown emitter BJT. The base current is stepped at 200uA per step. The vertical axis is 1mA/div. The current gain for this device, $\beta > 5$. The negative output resistance behavior of the collector current is due to internal heating of the device

IV. Regrown Emitter HBT

The motivation for the regrown emitter HBT is the lack of a need for an etch stop for the emitter mesa etch, and improved base contacts leading to lower parasitic base resistance and common emitter offset voltage. In addition, the regrown emitter HBT allows for more accurate base emitter junction placement than conventional structures grown by MOCVD because it is not subject to the Mg memory effect. The common emitter characteristics of a regrown emitter device in Figure 5 show a current gain of 6, a low offset voltage, and an early voltage, $V_A > 400V$. This preliminary result does not use a heterojunction emitter, suggesting that the current gain will be further improved in a regrown emitter HBT. The structure was grown by MOCVD on sapphire. The base thickness is 200 nm with an acceptor concentration, $N_A = 5\times10^{19}$, leading to a carrier concentration of $p = 8\times10^{17}cm^{-3}$. The emitter is GaN:Si, $N_D = 5\times10^{18}cm^{-3}$ 100 nm thick. The collector is 500 nm UID GaN with a background donor concentration of $N_D = 5\times10^{16}cm^{-3}$. The initial device growth consisted of the subcollector, collector, and base layers. An AlN_x dielectric mask is patterned with openings for the emitter structure (Figure 4). The emitter mesa is then grown selectively. The growth mask is removed, and device processing completed with the conventional Cl_2 RIE step to access the subcollector. Although attempts were made to selectively grow the emitter by MBE, these efforts have not yielded a working device. Photo-Electro-Chemical, PEC, wet etch techniques show promise for selectively etching n-type over p-type material[15], this etch would allow conventional processing of fully grown devices without the damage associated with the RIE etch. The etch stop becomes less effective, however, when the etch stop layer thickness, W_b is less than L_n, the diffusion length of electrons in the base - a necessary condition for transistor operation.

Although the regrown emitter device requires a regrowth interface in the base of the transistor, possibly leading to reduced transport or injection efficiency, it has achieved comparable current gain to etched emitter devices without the difficulties associated with the non-selective RIE emitter mesa etch and the base surface damage it causes. Circumventing these two major processing hurdles without degradation in performance makes the regrown emitter HBT a strong alternative to the conventional etched-emitter device.

V. HBT on LEO GaN

Both the regrown emitter and etched emitter structures suffer from of emitter collector leakage associated with threading dislocations(TDs). Due to the lattice mismatch between GaN and sapphire or SiC, thin GaN films ($\approx 2\ \mu m$) grown on these substrates have a TD density on the order of $5\times10^8\ cm^{-2}$. To investigate the connection between TDs, doping, and collector-emitter leakage currents, devices were fabricated on material grown using the lateral epitaxial overgrowth technique, LEO. The details of the LEO process are described by Fini et al [16]. LEO is well suited for this experiment because adjacent devices can be measured with and without dislocations. The window regions were 5 μm wide, repeated with a period of 40 μm. A full HBT structure is then grown on this sample by MBE. Over dislocated (window) regions the TDs continue, while over the wing regions, the lateral GaN growth is dislocation free. Figure 6 shows the spiral MBE growth indicative of TDs with screw character [17] in the window region, and the lack of this spiral growth mode on the wing regions. The devices tested had emitter mesa areas of $6\mu m \times 50\mu m$. The collector-emitter leakage of adjacent devices was tested (Figure 7) and was seen to drop by four orders of magnitude in the forward direction on the wing relative to the window. Common-emitter characteristics of an HBT on a wing region are shown in Figure 8. The gain of the wing device is comparable to devices in the window (dislocated) regions. This result suggests that although dislocations are the dominating cause of collector-emitter leakage in these devices, at the present levels ($10^8\ cm^{-2}$) they are not the cause of the high recombination rates in the base- which are expected to be related to the high Mg concentration ($10^{20}cm^{-3}$) and high levels of point defects. To our knowledge, this is the first demonstration of a GaN HBT on an LEO substrate. It conclusively demonstrates the connection between TDs and collector-emitter leakage.

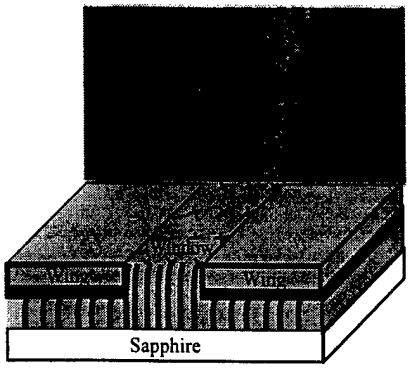

Fig. 6. Atomic Force Microscopy image of an LEO substrate (above) showing window and ring regions. Spiral growth mode in the window region is associated with the screw component of TDs. Wing regions consist of atomically flat steps.

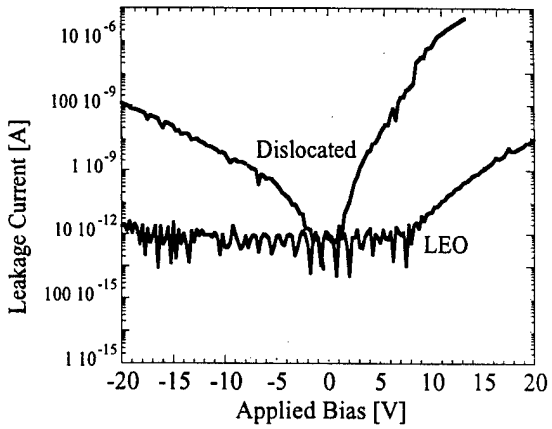

Fig. 7. Semi log plot of leakage current of LEO window compared to wing region. Plot shows reduction of leakage by four orders of magnitude for wing region as compared to window region. The emitter mesa area for these devices was 6 μmx 50 μm.

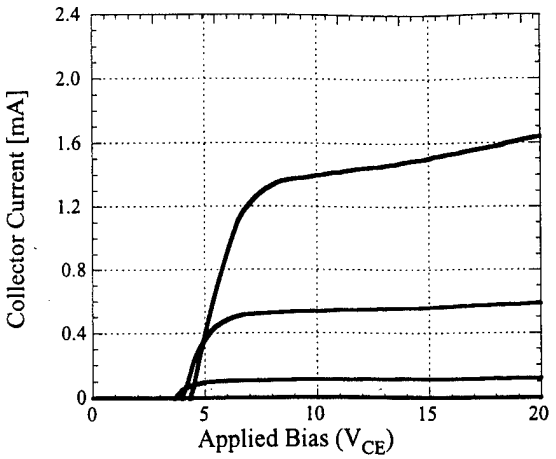

Fig. 8. Common emitter characteristics of GaN HBT on LEO wing (non-dislocated region). Base current steps are 400μA.

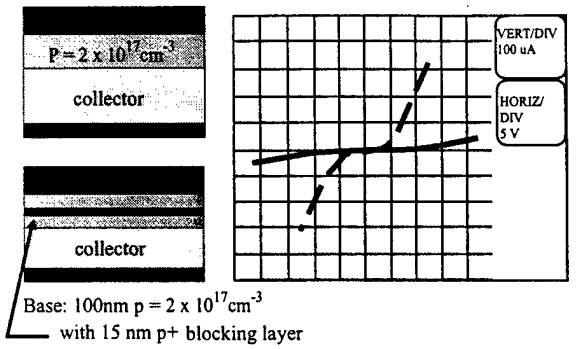

Fig. 9. Emitter-Collector leakage is reduced by the addition of a p+ spike in the neutral base of a transistor structure. The solid line represents the emitter-collector leakage of the device with the p^+ blocking layer, while the dashed line is corresponds to the device with a conventional base doped p=2×10^{17} cm^{-3}.

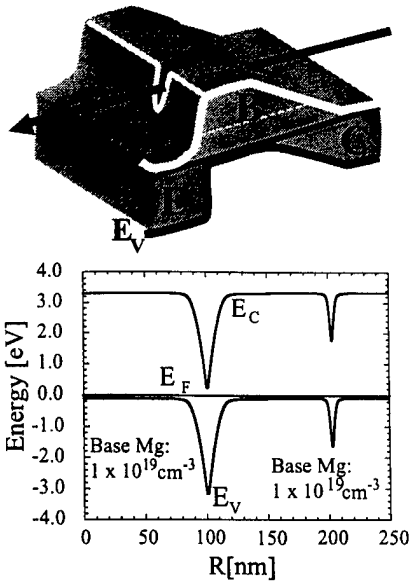

Fig. 10. **Above:** Three dimensional rendering of the band diagram of an HBT with a dislocation (arrow) causing local compensation of the p-type base. **Below:** Simulation of the band-diagram of a locally compensated area surrounding a dislocation in p-type GaN. A lightly doped base (left) is fully compensated near the dislocation, while a heavily doped base (right) is only partially compensated.

VI. Collector - Emitter Leakage Explained

A reoccurring problem with GaN HBTs has been the presence of significant collector-emitter leakage[5]. The GaN HBT on LEO (above) showed the connection between dislocations and leakage. The mechanism for collector-emitter leakage is found to be a localized punch-through effect. An experiment was performed in which two devices were fabricated, both with lightly doped bases ($N_A = 10^{19} \Rightarrow p = 10^{17}$ cm^{-3}) 100 nm thick, on areas of the same template with the approximately the same TD density (5×10^8 cm^{-2}). One of samples was grown with a 15 nm p^+ ($N_A = 10^{20} \Rightarrow p = 10^{18}$ cm^{-3}) spike in the center of the base to block emitter/collector leakage. The results of this experiment (Figure 10) show that the heavily doped spike in the neutral region of the base eliminated the emitter-collector short, suggesting that the mechanism for emitter-collector leakage is the local compensation of the base layer. The literature predicts that in n-type material TDs behave as electron traps, negatively charged when filled. In p-type material, the TDs are expected to behave as donors, or hole traps, and thus be positively charged[18]. Various energy levels have been predicted for midgap states associated with TDs ranging from 0.6 eV to 3.2 eV above the valence band[19]. Because the leakage was found to be dependent on both dislocation density and base doping, a hypothesis was developed for the mechanism of this leakage using the following model: We assume that each TD contributes a line of charge in p-type GaN equivalent to one donor for every 10Å vertically, or 10^7 cm^{-1}. We simulate this as a column doped n-type at 3×10^{20} cm^{-3} and having a radius of 1 nm. The donor level is taken to be 3 eV above the valence band edge. This level is chosen because it is consistent with a low-voltage punch through observed at lower doping levels, as well as the energetically favorable dislocation configuration in both Ga rich and N rich growth conditions[19]. Figure 9 shows the effect of the local compensation on the p-type base. The result of this compensation in extreme cases - $N_A = 10^{19}$ cm^{-3} is a device that is shorted from collector to emitter. When the base doping concentration is sufficiently high - $N_A = 10^{20}$ cm^{-3}, however, a barrier remains to prevent the short. Although in this case the dislocations were found to be the dominant source of emitter-collector leakage, it should be noted that surface states and mesa sidewall damage may lead to emitter-base and base-collector leakage currents in addition to the dislocation induced leakage paths.

VII. Collector-Emitter Leakage and DC Characteristics

Because the collector-emitter leakage mechanism is a localized punch-through effect, it is isolated from the base contact. This isolation results in the misleading situation in which both the base-emitter and base-collector diodes appear to be rectifying when tested individually, while in fact the active device is

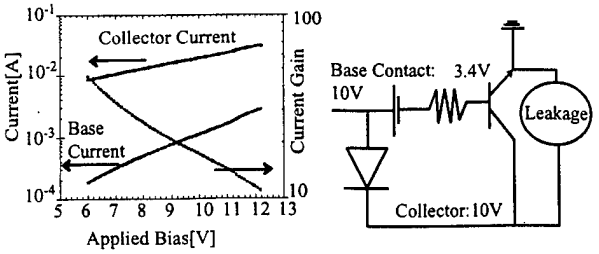

Fig. 11. Gummel plot of a bipolar transistor with emitter collector leakage. The current gain seems high, as the collector current is much greater than the base current. From the circuit diagram, however, we see an example bias condition where the collector-emitter voltage is large, even when V_{BC}=0. Figure 12 shows the common emitter characteristic for this device.

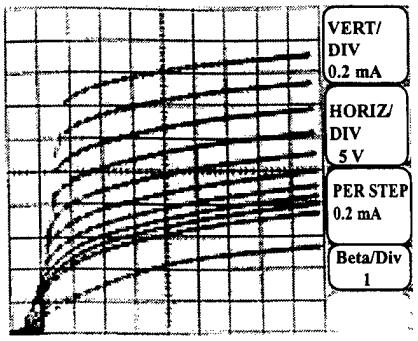

Fig. 12. Common emitter characteristics corresponding to Gummel plot in Figure 11 Current gain is actually much lower than predicted by the Gummel plot.

shorted. This short is not seen in the base emitter diode because an intact lateral p-n junction blocks the current from the p-base to the local punch-through region. It is not seen in the base-collector diode due to the Schottky barrier from the base contact to the compensated region. As described in Section III the high base contact resistance and lateral base resistance cause a disparity between the base voltage under the contact and under the emitter mesa. When combined with a collector-emitter leakage mechanism, this voltage disparity causes Gummel plots to be unreliable for the determination of current gain. For example, if the base-emitter *contact* voltage is 10V, and V_{CB} is set at zero, the actual collector-base voltage under the emitter mesa is 7V reverse, and the collector-emitter voltage is 10V. In devices that suffer from collector-emitter leakage, the forward current resulting from leakage may be greater than the current associated with the transistor action of the device. In this situation, the transistor current cannot be distinguished from the leakage current. A Gummel plot of a device with leakage current is shown in Figure 11. Although the Gummel plot suggests a current gain of 50, the common emitter characteristic for the same device, Figure 12, shows that the actual current gain is less than unity. Common base characteristics may also be misleading. This is because a collector-emitter leakage path will pass current without loss to the collector, and this may be misinterpreted as unity injection efficiency and transport. If the measurement is intended to demonstrate the transconductance of the device, care must be taken to drive the device with a voltage source rather than a current source. Transconductance is defined as $G_m = \partial I_C / \partial V_{BE}$. The parallel leakage path in the common base mode of the transistor may not be apparent when driven by a low output conductance current source, as the lower conductance of the source dominates. We conclude, therefore that when common-emitter characteristics are not useful due to emitter-collector leakage, common base and Gummel characteristics are not reliable in determining current gain.

VIII. Magnesium Memory Effect

The acceptor dopant most commonly used for p-type GaN is Magnesium. The Mg memory effect is common to many GaN MOCVD reactors. Etched-emitter devices are grown by MBE to avoid this problem. It is believed that due to the high Mg concentrations needed to adequately dope the p-type material, a substantial amount of Mg is left in an MOCVD reactor even after the flow is stopped. This Mg then incorporates into the film during subsequent growth. SIMS measurements of Mg levels in an NPN structure are shown in Figure 13. The plot shows a large Mg tail past the point where the Si is turned on and the Mg turned off. Because HBTs are especially sensitive to emitter-base junction placement[20], a growth technique which can accurately define these junctions is required. MBE growth eliminate these effects and enables the achievement of Mg doping profiles that are orders of magnitude sharper than in MOCVD grown GaN:Mg films. Another advantage of N_2 source MBE over MOCVD when growing Mg-doped GaN is that no post-growth anneal is required to electrically activate the Mg atoms. The absence of hydrogen in the plasma-assisted MBE process makes this unnecessary. Also, the structures grown by MBE typically have lower background impurity concentration which has resulted in extremely high electron mobilities at low temperature in AlGaN/GaN HEMT structures[21]. Finally, we have found the MBE growth to be more reproducible with greater uniformity across the sample.

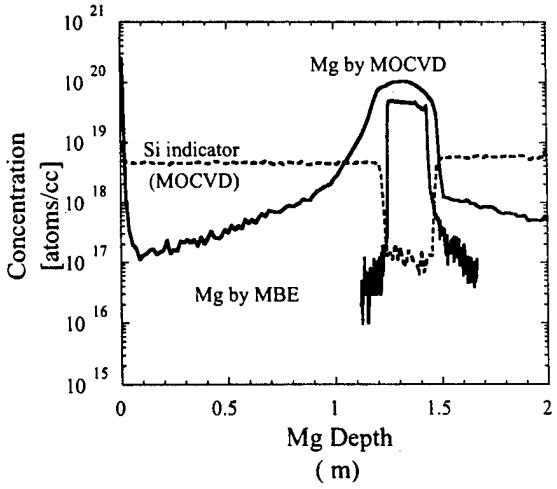

Fig. 13. SIMS study of Mg tail in the emitter of an MOCVD grown n-p-n structure compared with MBE grown junctions. In the MOCVD case, the second junction has been displaced by 170 nm past the point where the flow was stopped (coincident with the Si turn-on). For MBE the Mg turn-off is much more abrupt (2.5 nm/dec).

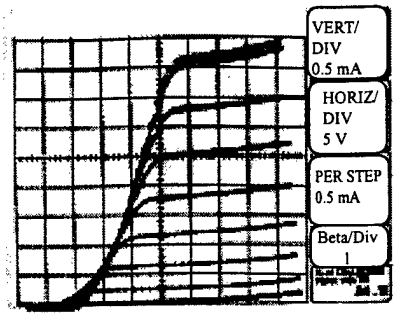

Fig. 14. Common Emitter characteristics of an HBT with 5% Al grading in the base. The current gain of this device is approximately 1.5, three times that of a similar device without the grade. Base current steps are 500μA/div. The collector current scale is 500μA/div.

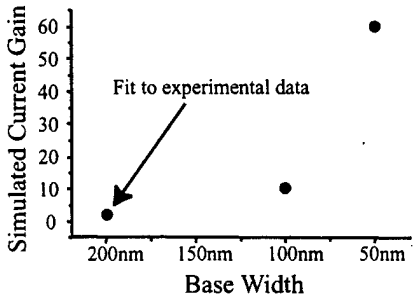

Fig. 15. Two-dimensional numerical simulation of current gain extrapolated from experimental data point as a function of base width. Simulation assumes that minority carrier lifetime in the neutral base is the limiting factor for current gain.

IX. Current Gain

The current gain of the GaN bipolar transistor is a major obstacle to the investigation of RF devices. The lifetime and the diffusivity of electrons in Mg doped GaN are unknown, but they are both expected to be low compared to practical base widths. This low lifetime is expected because of the high concentration of Mg in the base (between 5 and 10×10^{19} cm^{-3}) and high levels of point defects in Mg doped GaN[11]. Likewise, the electron velocity is expected to be adversely affected by the high base doping. Self consistent two-dimensional numerical simulations indicate the expected current gain as a function of base width (Figure 15). Although many key material properties in GaN are unknown, estimates can be used to gain useful insight into expected trends. For these simulations the electron lifetime used for the base was 25 ps. Minority carrier mobilities of μ_n=100 cm$^2/Vs$, μ_p=10 cm$^2/Vs$ and the effective masses, m_e=0.19 m_0, m_h= 0.6 m_0 were used. An advantage of AlGaN/GaN material system for HBTs is the large increase in bandgap with a relatively small Al composition:

$$E_g\,(AlN) - E_g\,(GaN) \approx 100 \cdot kT \qquad (6)$$

Suggesting that a compositional grade across the base of only 5% can result in an energy drop of 5kT. Assuming the acceptor level remains fixed relative to the valence band, this results in a quasi-field in the base of

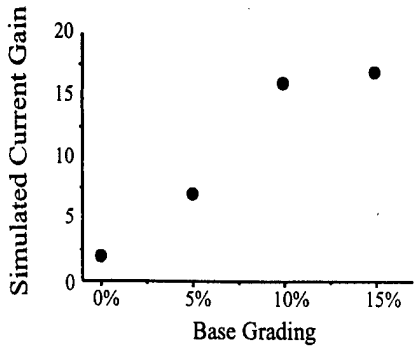

Fig. 16. Simulation of current gain enhancement as a function of base grading. Initial data point is experimental current gain value, and is used as a basis for the extrapolation for the data points with base compositional grading. The current gain is assumed to be limited by the minority carrier lifetime in the base, and is assumed not to be a function of Al composition.

$$\vec{E_q} = \frac{5 \cdot kT}{qW_b} \qquad (7)$$

For a 100nm base the quasi-field is then greater than 1.25×10^4 V cm^{-1}. Simulations reflecting this dependence of current gain with base compositional grading predict a dramatic increase in gain for modest grading (Figure 16). We have fabricated graded base devices and found some enhancement with Al compositional grading in the base (See Figure 14).

X. RF Device Characterization

Devices were grown using plasma assisted Molecular Beam Epitaxy (MBE) on templates grown by Metal Organic Chemical Vapor Deposition (MOCVD) on sapphire substrates. The device structure, Figure 17, consisted of a 500 nm GaN:Si (10^{18}cm^{-3}) subcollector followed by a 500 nm unintentionally doped (UID 1×10^{16}cm^{-3}) GaN collector.

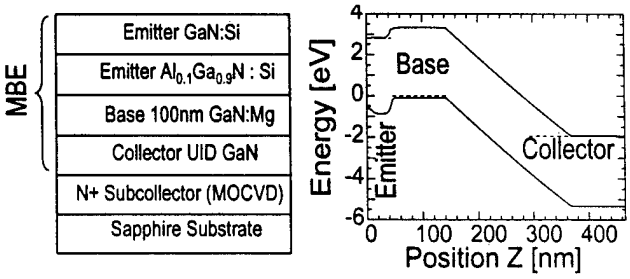

Fig. 17. Left: Structure for AlGaN/GaN HBT grown by plasma assisted MBE on MOCVD GaN on sapphire. The collector is unintentionally doped (UID) GaN $N_D \approx 10^{16}$cm^{-3}. Right: Simulated band diagram of typical device. The $Al_{0.1}Ga_{0.9}N$ heterojunction provides $\approx$10kT barrier to hole injection into the emitter.

The base was 100 nm GaN:Mg (5×10^{19}cm^{-3}) which due to the partial ionization of the Mg acceptors[11] leads to a hole concentration of 8×10^{17}cm^{-3}. Following the base layer is an abrupt heterojunction $Al_{0.1}Ga_{0.9}N$ (25 nm Si doped 3×10^{18}cm^{-3}) emitter capped with 5 nm of GaN:Si as a contact layer.

Because Mg is a deep acceptor in GaN, high Mg concentrations, $\approx 5\times10^{19}cm^{-3}$, are required to achieve hole concentrations in the base of $\approx 8\times10^{17}cm^{-3}$. In addition, the hole mobility in this material is low, $\approx$ 10 $cm^2/V\cdot s$. This resulted in a sheet resistivity of 100 kΩ/square in the 100 nm base of the device tested. High contact resistances complicate the problem, and fully ohmic contacts are difficult to achieve - especially on etched surfaces. The processing associated with the p-type base also presents several hurdles. Due to a lack of a reliable, controllable wet etch, a Cl_2 reactive ion etch (RIE) is conventionally used for etching AlGaN and GaN layers. Unfortunately, this etch does not stop on p-type layers, and damages the p-type surface, leading to poor contact quality. Also, the etch may lead to damaged sidewalls, contributing to base emitter leakage and high recombination rates at the emitter-base sidewall.

A. Device Fabrication

The devices were fabricated using Cl_2 RIE and standard liftoff metalization techniques as well as planarization and etch back techniques for the RF pad air bridge steps. Device fabrication consisted of an emitter mesa etch followed by base contact metalization (Pd/Au) and a base mesa etch. Collector and emitter contacts were then deposited (Ti/Al/Ni/Au). Next, a longer etch was used to isolate the devices to the sapphire substrate, and Cyclotene BCB was used to planarize device structures. A blanket CF_4+O_2 plasma etch was used to etch back the BCB and expose the emitter contact. Vias are then opened in the BCB exposing the base and collector contacts, and Ti/Au posts deposited. Contact pads were then deposited, completing the fabrication of the devices.

B. Electrical Characterization

DC and RF device characterization was performed on these devices. The DC current gain was found to be 3.5 with common emitter operation and low output conductance to 15 V (Figure 18). The low gain of these devices is thought to be associated with low minority carrier lifetimes in the base as well as sidewall recombination and possibly base-emitter leakage paths.

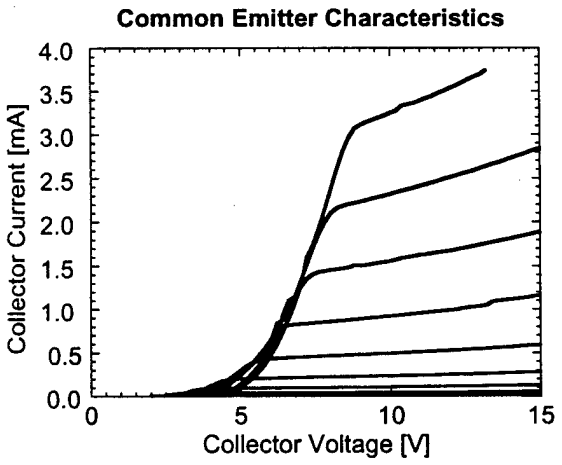

Fig. 18. Common Emitter characteristics of the 3x50 μmdevice. Base current is in steps of 250 μA.

The high offset voltage is associated with a large voltage drop across the base contact [?]. Small signal RF characterization with a vector network analyzer (VNA) from 50MHz to 10GHz showed agreement with DC gain measurements at 50MHz, with a 3dB reduction in the short circuit current gain (H_{21}) at 200 MHz and a roll off of approximately 10dB/decade. The current gain cutoff frequency was 2 GHz, although the response with frequency became nearly flat after 1 GHz (See Figure 19). This

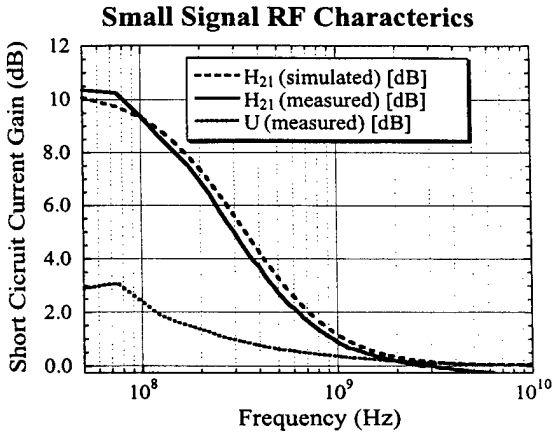

Fig. 19. Small signal short circuit current gain (H_{21}) and Mason's unilateral gain (U) of device. I_C=4 mA. Simulated curve is a small signal simulation of the equivalent circuit shown in Figure 20

non-ideal behavior of the device is thought to be due to the high sheet resistance of the base layer as well as high base contact resistances. The high resistance in the base leads to an equivalent circuit consisting of a distributed parasitic base-collector RC network which cannot be treated as a single RC time constant (Figure 20). The result is a continuum of time constants

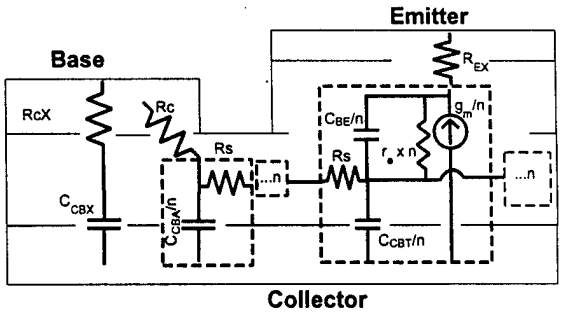

Fig. 20. Schematic of equivalent circuit of simulated circuit drawn on cross sectional diagram of device structure. Dashed boxes represent repeated blocks. Each block is repeated 'n=25' times. The element values used in the simulation were as follows: C_{CBX} = 0.4 pF, RcX =60 Ω. C_{CBA} = 50 fF, C_{BE} = 0.6 pF, C_{CBT} = 30 fF, R_S = 100 kΩ/square, $g_m=I_E/V_T$ = 350 mS, re = 3 Ω.

which together lead to a reduction of H_{21} of $\approx$ 10 dB/decade in frequency as opposed to the usual 20 dB/decade. To confirm the plausibility of this model, a finite element small signal equivalent circuit simulation was carried out using HP ADS. A representation of the simulated circuit is shown in Figure 20 and the

result plotted in Figure 19. A diagram of the relevant geometries of the device are shown in Figure 21.

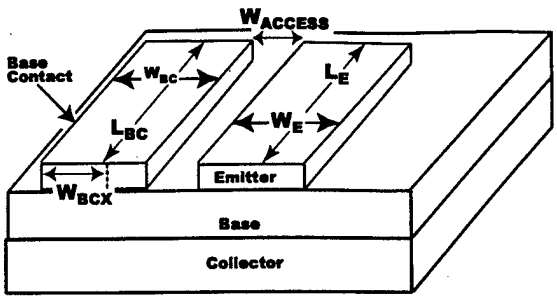

Fig. 21. Diagram of the device geometry for the AlGaN/GaN HBT and the geometry used to model the small signal RF response of the device. Device dimensions are as follows (in microns): W_E =3, L_E = 50 , W_{Access} = 1, W_{BC} = 9, W_{BCX} = 8, L_{BC} = 72.

To model the distributed nature of the device, the active and access blocks are repeated 25 times (as indicated in Figure 20). C_{CBX} = 0.4 pF represents the capacitance under the extrinsic base contact, and is in series with a vertical contact resistance, RcX = 60 Ω. C_{BC} also has a component in the access region to the base (C_{CBA} = 50 fF). Active device blocks contain a hybrid-pi small signal equivalent circuit element with a base-emitter capacitance (C_{BE} = 0.6 pF) and a base-collector capacitance element (C_{CBT} = 30 fF). The access and active blocks are connected by a sheet resistance, R_S = 100 kΩ/square. The small signal transconductance, g_m used was I_E/V_T = 350 mS, where V_T is the thermal voltage, 26 mV, and the emitter current, I_E was 9 mA. The values used in the simulation represent a measured R_s in the base, I_E, and approximate (within 5%) lumped capacitance values calculated from the geometry of the device. There were several adjustable parameters due to the difficulty in measuring a non-linear base contact resistance, R_{CX}, R_C, as well as an unknown emitter resistance, R_{EX} and unknown forward transit time (τ_F), where:

$$C_{BE} = C_{BE\ \text{Diffusion}} + C_{BE\ \text{Depletion}} \quad (8)$$

$$C_{BE\ \text{Diffusion}} = \tau_F \cdot g_m \quad (9)$$

Due to the many adjustable parameters, it is difficult to assert the correlation between all the values chosen for the simulation and actual device parasitics. It can be concluded, however, that the distributed finite element model gives a plausible explanation for the response of the device.

XI. Conclusions and Future Work

Calculations based on material properties show the great potential of the GaN HBT. Technological barriers to the realization of this potential include low base conductivity, the deep acceptor- Mg, emitter collector leakage currents, and short electron lifetimes in the base. Selective area regrowth of base contact areas has demonstrated improvement of the extrinsic base conductivity, while emitter mesa regrowth was used to avoid etch damage, which is known to degrade base contacts. The use of LEO templates for HBTs has demonstrated the need for low dislocation densities in GaN for HBTs, and doping studies have confirmed the compensating nature of these dislocations in p-type GaN. Aluminum compositional grading in the base of an AlGaN/GaN HBT is expected to enhance carrier transport across the base, and common-emitter characteristics of a graded base device were presented. It is expected that for high frequency operation, the emitter stripe width, base thickness, base-emitter access length, and base contact size must all be reduced significantly. Furthermore, the base contact resistance as well as the base sheet resistance must be reduced to attain power gain from this device. We conclude, therefore, that although the development of the AlGaN/GaN HBT faces significant technological obstacles, the potential viability for an RF device has been demonstrated, suggesting a direction for further development. Future efforts will be concentrated on improving current gain and reducing base contact and bulk resistance.

References

[1] Y. F. Wu, B. P. Keller, S. Keller, J. J. Xu, B. J. Thibeault, S. P. DenBaars, and U. K. Mishra, "GaN-based FETs for microwave power amplification" *IEICE Trans. Electron. (Japan)*, vol. E82-C, no. 11, pp. 1895–905, 1999.

[2] L. S. McCarthy, P. Kozodoy, M. J. W. Rodwell, S. P. DenBaars, and U. K. Mishra "AlGaN/GaN heterojunction bipolar transistor," *IEEE Electron Device Lett. (USA)*, vol. 20, no. 6, pp. 277–9, 1999.

[3] J. B. Limb, H. Xing, B. Moran, L. McCarthy, S. P. DenBaars, and U. K. Mishra, "High voltage operation (> 80 V) of GaN bipolar junction transistors with low leakage," *Appl. Phys. Lett. (USA)*, vol. 76, no. 17, pp. 2457–9, 2000.

[4] S. Yoshida and J. Suzuki, "Characterization of a GaN bipolar junction transistor after operation at 300 degrees C for over 300 h," *Jpn. J. Appl. Phys. 2, Lett. (Japan)*, vol. 38, no. 8A, pp. L851–3, 1999.

[5] B. S. Shelton, J. J. Huang, D. J. H. Lambert, T. G. Zhu, M. M. Wong, C. J. Eiting, H. K. Kwon, M. Feng, and R. D. Dupuis, "AlGaN/GaN heterojunction bipolar transistors grown by metal organic chemical vapor deposition," *Electron. Lett. (UK)*, vol. 36, no. 1, pp. 80–1, 2000.

[6] S. Nakamura, "Development of violet InGaN-based laser diodes," *Oyo Buturi (Japan)*, vol. 68, no. 7, pp. 793–6, 1999.

[7] " High-performance (Al,Ga)N-based solar-blind ultraviolet p-i-n detectors on laterally epitaxially overgrown GaN," G. Parish, S. Keller, P. Kozodoy, J. P. Ibbetson, H. Marchand, P. T. Fini, S. B. Fleischer, S. P. DenBaars, U. K. Mishra, and E. J. Tarsa *Appl. Phys. Lett. (USA)*, vol. 75, no. 2, pp. 247–9, 1999.

[8] U. V. Bhapkar and M. S. Shur, "Monte Carlo calculation of velocity-field characteristics of wurtzite GaN," *J. Appl. Phys. (USA)*, vol. 82, no. 4, pp. 1649–55, 1997.

[9] J. Kolnik, I. H. Oguzman, K. F. Brennan, Wang Rongping, and P. P. Ruden, "Monte Carlo calculation of electron initiated impact ionization in bulk zinc-blende and wurtzite GaN," *J. Appl. Phys. (USA)*, vol. 81, no. 2, pp. 726–33, 1997.

[10] Q. Lee, S. C. Martin, D. Mensa, R. P. Smith, J. Guthrie, S. Jaganathan, T. Mathew, S. Krishnan, S. Creran, and M. J. W. Rodwell, "Submicron transferred-substrate heterojunction bipolar transistors with greater than 8000 GHz f/sub max," in *Proc. IPRM*, 1999, pp. 175–8.

[11] P. Kozodoy, H. Xing, S. P. DenBaars, U. K. Mishra, A. Saxler, R. Perrin, S. Elhamri, and W. C. Mitchel, "Heavy doping effects in Mg-doped GaN," *J. Appl. Phys. (USA)*, vol. 87, no. 4, pp. 1832–5, 2000.

[12] H. Katayama-Yoshida, T. Nishimatsu, T. Yamamoto, and N. Orita, "Codoping in wide band-gap semiconductors," in *Proc. ISCS*,1998, pp. 747–56,

[13] J. S. Im, A. Moritz, F. Steuber, V. Harle, F. Scholz, and A. Hangleiter, "Radiative carrier lifetime, momentum matrix element, and hole effective mass in GaN," *Appl. Phys. Lett.*, vol. 70, no. 5, pp. 631–3, 1997.

[14] Jang Ja-Soon, Park Seong-Ju, and Seong Tae-Yeon "Formation of low resistance Pt ohmic contacts to p-type GaN using two-step surface treatment," *J. Vac. Sci. Technol. B, Microelectron. Nanometer Struct. (USA)*, vol. 17, no. 6, pp. 2667–70, 1999.

[15] A R Stonas, P Kozodoy, H Marchand, P Fini, S Keller, S P DenBaars, U K Mishra, and E L. Hu, ,"Backside-illuminated photoelectrochemical etching for the fabrication of deeply undercut GaN structures," *Appl. Phys. Lett.* , vol.77, no.16, p.2610-12, 2000.

[16] P. Fini, L. Zhao, B. Moran, M. Hansen, H. Marchand, J. P. Ibbetson, S. P. DenBaars, U. K. Mishra, and J. S. Speck, "High-quality coalescence of

laterally overgrown GaN stripes on GaN/sapphire seed layers," *Appl. Phys. Lett. (USA)*, vol. 75, no. 12, pp. 1706–8, 1999.

[17] B. Heying, E. J. Tarsa, C. R. Elsass, P. Fini, S. P. DenBaars, and J. S. Speck, "Dislocation mediated surface morphology of GaN," *J. Appl. Phys. (USA)*, vol. 85, no. 9, pp. 6470–6, 1999.

[18] K. Leung, A. F. Wright, and E. B. Stechel, "Charge accumulation at a threading edge dislocation in gallium nitride," *Appl. Phys. Lett. (USA)*, vol. 74, no. 17, pp. 2495–7, 1999.

[19] Lee Seung Mi, M. A. Belkhir, Zhu Xiao Yan, Lee Young Hee, Hwang Yong Gyoo, and T. Frauenheim, "Electronic structures of GaN edge dislocations," *Phys. Rev. B, Condens. Matter (USA)*, vol. 61, no. 23, pp. 16033–9, 2000.

[20] S. M. Sze, *Physics of semiconductor devices*, Wiley, New York, 2nd edition, 1981.

[21] C. R. Elsass, I. P. Smorchkova, B. Heying, E. Haus, P. Fini, K. Maranowski, J. P. Ibbetson, S. Keller, P. M. Petroff, S. P. DenBaars, U. K. Mishra, and J. S. Speck, "High mobility two-dimensional electron gas in AlGaN/GaN heterostructures grown by plasma-assisted molecular beam epitaxy," *Appl. Phys. Lett. (USA)*, vol. 74, no. 23, pp. 3528–30, 1999.